



ELSEVIER

Available online at www.sciencedirect.com

ScienceDirect

Acta Materialia 94 (2015) 152–161

**Acta** MATERIALIA

www.elsevier.com/locate/actamat

A geometric model for intrinsic residual strain and phase stability in high entropy alloys

Y.F. Ye, C.T. Liu and Y. Yang*

Centre for Advanced Structural Materials, Department of Mechanical and Biomedical Engineering, City University of Hong Kong, Tat Chee Avenue, Kowloon Tong, Kowloon, Hong Kong, China

Received 28 January 2015; revised 12 April 2015; accepted 19 April 2015

Available online 19 May 2015

Abstract—Following the Hume–Rothery rules, it is a longstanding notion that atomic size mismatch induces intrinsic residual strains in a common lattice which may cause lattice instability and thus phase transition in an alloy. For conventional alloys, such an intrinsic residual strain can be derived with the continuum theory of elasticity; however, lack of distinction between solvent and solute atoms in recently developed high entropy alloys simply defies such an approach. Here, we develop a general self-contained geometric model that enables the calculation of intrinsic residual strains around different sized elements in a multi-component alloy, which links the average lattice constant of the alloy to a few critical geometric variables related to the close atomic packing in that lattice, such as atomic size, atomic fraction and packing density. When applied to glass-forming high entropy alloys and bulk metallic glasses, our model unravels that amorphization occurs when the root-mean-square (R.M.S.) residual strain rises above ~10%, in good agreement with the Lindemann's lattice instability criterion. By comparison, the transition from a single- to multi-phase solid solution takes place in crystalline high entropy alloys when the R.M.S. residual strain approaches ~5%. Our current findings provide a quantitative insight into phase stability in multicomponent alloys, which should be useful in the design of high entropy alloys with desired phases.

© 2015 Acta Materialia Inc. Published by Elsevier Ltd. All rights reserved.

Keywords: High entropy alloys; Analytical modeling; Hume–Rothery's rules; Metal and alloys; Phase stability

1. Introduction

Alloying different types of atoms in a common lattice has been an efficient way to make alloys with improved structural/functional properties. Since the ancient times, human beings have made tremendous efforts in the development of alloys with desired phases, and also in the search of an efficient method that can guide us in finding the compositions of such alloys. Among the early efforts, one important finding is the set of Hume–Rothery rules that were established in the 1920s for the conditions under which an element can dissolve into a metal to form a solid solution [1]. According to the Hume–Rothery rules [1], the stability of a solid solution is controlled by three major factors, i.e. the atomic size, the electronegativity difference and the electron concentration effect. When applied to binary alloys, these rules state that the formation of a primary solute solution is favored if the following conditions are met: (1) the ratio of the Goldschmidt radii of two constituent atoms is between 0.8 and 1.2 or the atomic size difference is less than ~15%; (2) the difference in their Pauling electronegativity is small; and (3) the electron concentration

or the total number of valence electrons (VEC) is in a proper range [1].

The physical understanding of the Hume–Rothery rules has been a longstanding research topic in the classic field of metallurgy [1]. While mechanisms proposed for the 2nd and 3rd rules are still debated, the mechanism underlying the 1st rule, i.e. the atomic size rule, was well established, which can be related to the elastic energy of a solid solution [2] or equivalently the atomic level stress occurring in different sized atoms [3–5], which tends to destabilize a crystal structure after being built up to a critical level. By treating solute atoms alloyed with solvent atoms as a sphere-in-hole problem, the elastic theory of the atomic size effect was advanced by Eshelby in the 1950s [2], according to which a tolerable atomic size difference was predicted to be less than 15% for the formation of a binary solid solution. Alternatively, the atomic size effect can be also rationalized with the atomic stress theory proposed by Egami and co-workers [3–5]. According to this atomic stress theory [4], mixing of two sized atoms together brings about atomic stresses, the magnitude of which scales with the atomic size difference. When the volumetric strain resulting from the atomic stresses reaches a critical value [3,5], the crystal structure becomes unstable and therefore shows a tendency to turn into an amorphous structure. In other words, the atomic stress theory suggests that one needs to keep a

* Corresponding author. Tel.: +852 34429394; fax: +852 34420172; e-mail: yonyang@cityu.edu.hk

low atomic size ratio for retaining the solid solution crystalline structure in a binary alloy, which is consistent with the Hume–Rothery rule as backed by the elasticity theory of Eshelby [2].

Now let us discuss high entropy alloy (HEA), which offers the motivation of the current work and is loosely defined as the multicomponent alloy with at least five elements mixed in equal or nearly equal molar fractions [6–12]. Despite the relatively large number of constituent elements in HEAs as compared to ordinary alloys, a great number of experiments revealed that, upon solidification, some HEAs tend to form single- or multi-phased solid solutions rather than intermetallics [7,10–15]; while some others tend to form metallic glasses as metastable structures [8,9,11,15]. To understand such phase diversities in HEAs, several empirical rules were put forward, such as the modified VEC rule [14,16] and the variety of atomic size difference rules [11,15,17,18], which are similar to the original Hume–Rothery rules. Although some of these newly proposed empirical rules are seemingly applicable to HEAs, the underlying physical mechanisms however are still debated. Following the similar line of reasoning as for the Hume–Rothery rules, it was once proposed that mixing of different sized elements would cause a high residual strain and thus phase transition in HEAs [6,17]. Nevertheless, as of today, there still lacks a theoretical model to evaluate the residual strain in HEAs, despite its fundamental importance and technologic relevance to the design of these newly developed alloys.

Conceptually, the equiatomic composition of HEAs defies the direct use of the Eshelby's elasticity approach in calculating the residual strain because one cannot simply define the solvent ("matrix") atoms versus the solute ("inclusion") atoms in HEAs. To circumvent this difficulty, here we propose a geometric approach, which is based on the fact that most of the HEAs display well-defined lattice structures, such as fcc and bcc, with very sharp X-ray or neutron diffraction peaks like ordinary alloys [6,7,10,12–14,19]. In such a case, if atoms still remain in close packing in HEAs just like in ordinary alloys, one can then infer that the different sized atoms need to be "squeezed-in" or "stretched-out" in order to retain a common lattice. Otherwise, atomic packing misfit could arise throughout the whole lattice(obviously, a large atom can always be closely packed with more neighbors than a small one), which defies the establishment of a long-range periodic lattice structure with a uniform packing density and contradicts the diffraction spectra of HEAs that indicate well-behaved lattice structures similar to those in conventional alloys [6,7,10,12–14,19]. In other words, to avoid atomic packing misfit, the sizes of the constituent atoms in HEAs must be adjusted and differ from those in pure metals. Indeed, it was noticed decades ago that the apparent atomic size of an element changes with alloying [20], which was then thought to be caused partly by residual strains and partly by the alteration in the electronic structures of elements. For the current work, we focus on the atomic size effect alone while neglecting the other possible effects, such as the Pauling electronegativity and VEC effect. In such a sense, the residual strain as derived from our model provides an upper-bound estimate due to the neglect of these chemical effects. In what follows, we first develop a general self-contained geometric model that can enable us to calculate the residual strain in multi-component alloys; after that, we apply this model to study phase stability in many different types of

alloys, such as bulk metallic glasses and HEAs; finally, based on the comparison of our theoretical model and the experimental data, we would discuss the possible mechanisms of phase transition in HEAs.

2. Theoretical modeling

2.1. A geometric model

To quantify the local atomic packing efficiency, we adopt the concept of the three-dimensional solid angle as illustrated in Fig. 1(a), which can be generally expressed as $\omega = 2\pi(1 - \cos \theta)$ [21], where θ denotes the semi-angle of the cone [Fig. 1(a)]. For the solid angle ω_{ij} subtended by the atom j around the central atom i , we have:

$$\omega_{ij} = 2\pi \left[1 - \frac{\sqrt{r_i(r_i + 2r_j)}}{r_i + r_j} \right] \quad (1)$$

where r denotes the atomic radius. Following the atomic stress theory [4], the atomic packing efficiency η_i of the central atom i can be expressed as:

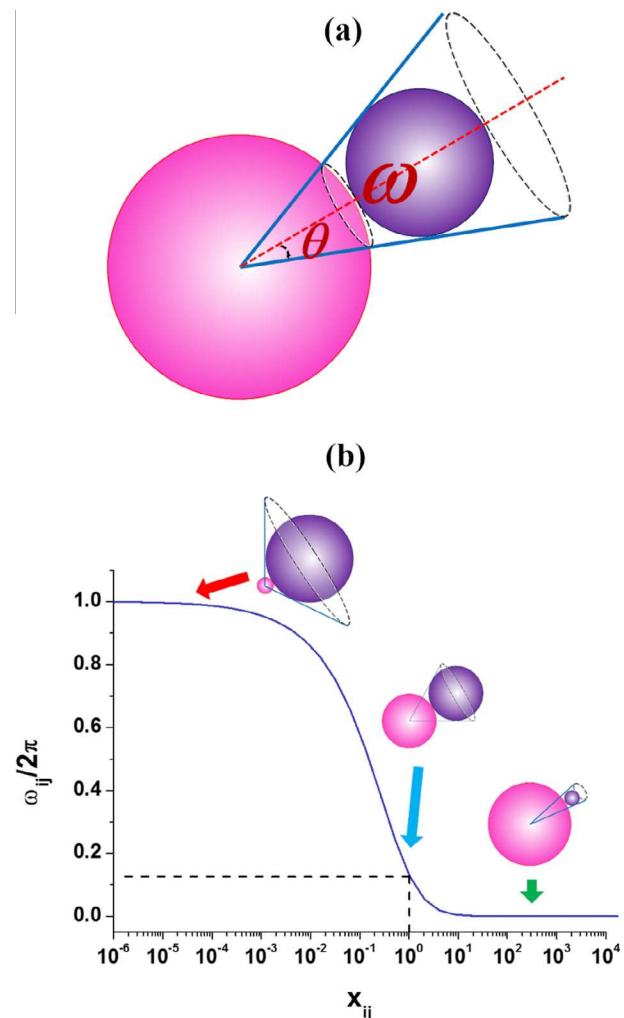


Fig. 1. (a) The schematic of the three-dimensional (3D) solid angle defined for the two spheres in direct contact, and (b) the variation of the solid angle $\omega_{ij}/2\pi$ with the atomic size ratio x_{ij} .

$$\eta_i = \frac{N_i \sum_{j=1}^n c_j \omega_{ij}}{4\pi} = \frac{N_i}{2} \sum_{j=1}^n c_j \left[1 - \frac{\sqrt{x_{ij}(x_{ij}+2)}}{x_{ij}+1} \right] \quad (2)$$

Here the denominator 4π corresponds to the solid angle of a unit sphere; c_j is the probability of having the atom j as the nearest neighbor of the central atom; N_i is the coordinate number (CN) of the central atom i and the atomic size ratio $x_{ij} = r_i/r_j$. Note that the atomic packing efficiency derived based on the solid angle concept can be used to define an atomic size parameter which can be related to the phase stability in multicomponent alloys, as discussed in Ref. [18]. As seen in Fig. 1(b), the solid angle ω_{ij} decreases with the increasing atomic size ratio, approaching $\omega_{ij} = 2\pi$ for $x_{ij} \sim 0$, $\omega_{ij} = 0.63$ for $x_{ij} \sim 1$ and $\omega_{ij} = 0$ for $x_{ij} \gg 1$. Given the wide range of element size one can choose for a HEA, it can be pictured that the local atomic packing efficiency could vary dramatically if there were no residual strains, which leads to a “distorted” lattice as illustrated in Figs. 2(a). However, the “distorted” lattice does not yield sharp diffraction peaks as exhibited by HEAs; therefore, the atoms must be “stretched” or “squeezed”, leading to the atomic size alteration as noticed by King in the 1960s [20]. In theory, the change in the atomic size gives rise to the local residual strain, as illustrated in Fig. 2(b).

Assuming that the atomic packing efficiency η_i reaches an equilibrium value of $\bar{\eta}$ after the alteration of the size of an atom as well as its local coordination number (CN), we can derive (please see Appendix A.1 for details):

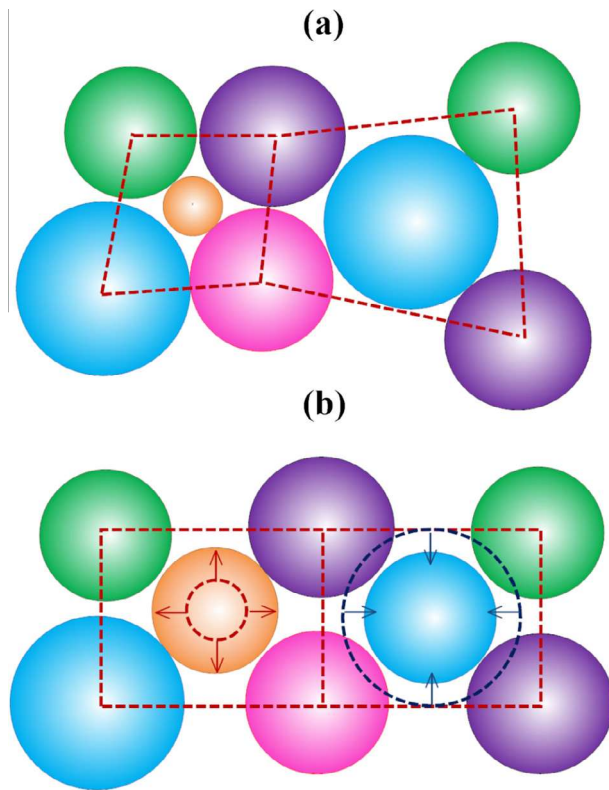


Fig. 2. The schematics of (a) the “distorted” lattice comprised of closely packed atoms without lattice strains and (b) the well-behaved lattice comprised of closely packed atoms with lattice strains. Note that the dashed circles denote the profile of the original atom and the arrows indicate the direction of the residual strain.

$$\bar{\eta} = \eta_i + \delta\eta_i = \frac{N_i \sum_{j=1}^n c_j (\omega_{ij} + \delta\omega_{ij}) + \delta N_i \sum_{j=1}^n c_j \omega_{ij}}{4\pi} \quad (3)$$

where δ denotes the incremental change of a physical quantity; $\delta\omega_{ij} = -A_{ij}(\varepsilon_i - \varepsilon_j)$ in which $A_{ij} = \frac{2\pi x_{ij}}{(x_{ij}+1)^2 \sqrt{x_{ij}(x_{ij}+2)}}$ and the residual strain $\varepsilon_i = \frac{\delta r_i}{r_i}$. Furthermore, the total volume of the alloy should remain constant after the development of these residual strains, which requires that the average residual strain is zero, namely, $\langle \varepsilon \rangle = \sum_{j=1}^n c_j \varepsilon_j = 0$.

Based on the above considerations, we can obtain:

$$\varepsilon_i = \left(1 + \frac{\delta N_i}{N_i} \right) \frac{\sum_{j=1}^n \omega_{ij} c_j}{\sum_{k=1}^n A_{ik} c_k} - \frac{4\pi \bar{\eta}}{N_i \sum_{k=1}^n A_{ik} c_k} \quad (4)$$

Note that Eq. (4) corresponds to the general case that the CN of a central atom changes with the intrinsic residual strain. However, for the special case of a single-phase random solid solution, the CN can be regarded as a constant and the probability c_j should be equal to the atomic fraction of the j th element. In such a case, Eq. (4) can be simplified as:

$$\varepsilon_i = \frac{\sum_{j=1}^n \omega_{ij} c_j}{\sum_{k=1}^n A_{ik} c_k} - \frac{4\pi \bar{\eta}}{N_i \sum_{k=1}^n A_{ik} c_k} \quad (5)$$

Next, let us derive one possible expression for $\bar{\eta}$ in order to calculate ε_i . For this purpose, we turn to the lattice constant a_n of an n -element alloy. With the presence of the intrinsic residual strains ε_i ($i = 1, 2, \dots, n$), we can simply write $a_n = \sum_{i=1}^n a_i c_i (1 + \varepsilon_i)$ based on the rule of mixture, where a_i is the constant of the lattice made up of the i th element. Substituting Eq. (5) into this equation then gives:

$$a_n = \sum_{i=1}^n a_i c_i + \sum_{i=1}^n \left(a_i c_i \frac{\sum_{j=1}^n c_j \omega_{ij}}{\sum_{k=1}^n c_k A_{ik}} \right) - \frac{4\pi \bar{\eta}}{N} \sum_{i=1}^n \left(\frac{a_i c_i}{\sum_{j=1}^n c_j A_{ij}} \right) \quad (6)$$

Note that the first term on the right hand side (R.H.S.) of Eq. (6) corresponds to the classic Vegard's law [22]: $a_n = \sum_{i=1}^n a_i c_i$, the second term to the scenario of lattice expansion (due to the insertion of large sized atoms) while the third term to the scenario of lattice contraction (due to structural relaxation into an equilibrium packing configuration). Note that Eq. (6) indicates the lattice constant a_n of a multicomponent alloy could be either larger or smaller than the prediction of the Vegard's law, which agrees with the experimental findings as reported in Refs. [23–25]. With Eq. (6), we can now extract the equilibrium packing fraction $\bar{\eta}$ if the lattice constant a_n of a multicomponent alloy is known a priori and, subsequently, be able to compute the intrinsic residual strains using Eq. (5).

2.2. Ideal atomic packing fraction

By using the experimentally determined lattice constant as the input, we can now calculate the equilibrium packing fraction $\bar{\eta}$ and the intrinsic residual strain around each element in an alloy with Eqs. (5) and (6). However, this is still inconvenient for the development of new alloys whose lattice constants are most likely unknown. For such cases, it would be useful if we could derive an analytic expression for the equilibrium packing fraction $\bar{\eta}$. Here, we propose

that the equilibrium packing fraction $\bar{\eta}$ may be approximated by an ideal atomic packing fraction η_{ideal} , which is simply the weighted average of the ideal packing fractions η_i of the constituent elements without the intrinsic residual strains, namely:

$$\bar{\eta} \approx \eta_{ideal} = \sum_{i=1}^n c_i \eta_i = \frac{1}{2} \sum_{i=1}^n \sum_{j=1}^n c_j c_i N_i \left[1 - \frac{\sqrt{x_{ij}(x_{ij} + 2)}}{x_{ij} + 1} \right] \quad (7)$$

To verify Eq. (7), we performed an extensive study of the alloys with a random solid solution structure, including the binary alloys whose lattice constants are achieved in the literature [26] and some multicomponent HEAs whose lattice constants were recently obtained through

experiments. The experimental and calculation results are all tabulated in Table I. For the sake of comparison, the lattice constants a_v predicted by the Vegard's law are also included. Note that the atom size of different elements used for the theoretical calculation was all taken from Ref. [15]. Here, the values of $\bar{\eta}$ are extracted from the experimental data a_{exp} according to Eq. (6) while those of η_{ideal} are computed using Eq. (7). As seen in Table I, it is evident that the magnitude of the ideal packing fraction η_{ideal} is very close to that of the equilibrium packing fraction $\bar{\eta}$, within a relative error of less than 2%. This important finding indicates that, to the first order approximation, one may safely take the equilibrium packing fraction $\bar{\eta}$ to be the ideal packing fraction η_{ideal} for the alloys of random solid solution.

Table I. The summary of the experimentally determined lattice constants of different alloys in comparison to the predictions from the Vegard's law together with the extracted equilibrium packing fractions $\bar{\eta}$ in comparison to the ideal packing fractions η_{ideal} .

Composition	Phase	a_{exp} (Å)	a_v (Å)	$\bar{\eta}$	η_{ideal}	$ (\bar{\eta} - \eta_{ideal})/\eta_{ideal} $ (%)	Reference
Cu _{77.9} Au _{22.1}	fcc	3.737	3.717	0.797	0.805	1.02	[26]
Cu ₇₅ Au ₂₅	fcc	3.754	3.731	0.796	0.805	1.17	[26]
Cu _{69.8} Au _{30.2}	fcc	3.778	3.755	0.796	0.806	1.22	[26]
Cu ₆₅ Au ₃₅	fcc	3.809	3.777	0.794	0.806	1.50	[26]
Cu ₅₀ Au ₅₀	fcc	3.873	3.847	0.795	0.806	1.38	[26]
Cu _{33.3} Au _{66.7}	fcc	3.948	3.924	0.796	0.806	1.21	[26]
Cu _{25.7} Au _{74.3}	fcc	3.981	3.959	0.797	0.805	1.06	[26]
Au _{89.6} Ag _{10.4}	fcc	4.077	4.080	0.804	0.804	0.06	[26]
Au _{68.7} Ag _{31.3}	fcc	4.076	4.081	0.805	0.804	0.15	[26]
Au ₅₀ Ag ₅₀	fcc	4.076	4.083	0.805	0.804	0.18	[26]
Au _{35.5} Ag _{64.5}	fcc	4.078	4.084	0.805	0.804	0.17	[26]
Au _{22.5} Ag _{77.5}	fcc	4.080	4.085	0.805	0.804	0.13	[26]
Au _{9.1} Ag _{90.9}	fcc	4.083	4.086	0.805	0.804	0.10	[26]
Al _{99.41} Mg _{0.59}	fcc	4.051	4.053	0.804	0.804	0.04	[26]
Al _{98.81} Mg _{1.19}	fcc	4.053	4.056	0.804	0.804	0.06	[26]
Al _{97.79} Mg _{2.21}	fcc	4.058	4.061	0.804	0.804	0.03	[26]
Al _{95.52} Mg _{4.48}	fcc	4.068	4.072	0.804	0.804	0.00	[26]
Al _{93.28} Mg _{6.72}	fcc	4.078	4.082	0.804	0.804	0.02	[26]
Al _{90.99} Mg _{9.01}	fcc	4.088	4.093	0.804	0.804	0.05	[26]
Al _{88.8} Mg _{11.2}	fcc	4.099	4.104	0.804	0.805	0.11	[26]
Al _{86.7} Mg _{13.3}	fcc	4.108	4.114	0.804	0.805	0.13	[26]
Al _{84.4} Mg _{15.6}	fcc	4.118	4.125	0.804	0.805	0.12	[26]
Fe _{29.89} Co _{70.11}	bcc	2.843	2.882	0.544	0.536	1.48	[26]
Fe _{39.66} Co _{60.34}	bcc	2.848	2.880	0.542	0.536	1.18	[26]
Fe _{49.7} Co _{50.3}	bcc	2.855	2.878	0.541	0.536	0.86	[26]
Fe _{59.51} Co _{40.49}	bcc	2.860	2.875	0.539	0.536	0.58	[26]
Fe _{69.56} Co _{30.44}	bcc	2.864	2.873	0.538	0.536	0.32	[26]
Fe _{79.52} Co _{20.48}	bcc	2.867	2.871	0.537	0.536	0.14	[26]
Fe _{89.27} Co _{10.73}	bcc	2.867	2.868	0.536	0.536	0.06	[26]
Mo _{88.8} Ta _{11.2}	bcc	3.160	3.165	0.537	0.536	0.11	[26]
Mo _{74.8} Ta _{25.2}	bcc	3.181	3.187	0.537	0.536	0.11	[26]
Mo _{65.2} Ta _{34.8}	bcc	3.192	3.202	0.537	0.536	0.22	[26]
Mo _{55.9} Ta _{44.1}	bcc	3.207	3.216	0.537	0.536	0.19	[26]
Mo _{46.2} Ta _{53.8}	bcc	3.221	3.231	0.537	0.536	0.21	[26]
Mo _{32.5} Ta _{67.5}	bcc	3.244	3.252	0.537	0.536	0.19	[26]
Mo _{19.2} Ta _{80.8}	bcc	3.269	3.273	0.536	0.536	0.05	[26]
CoCrFeNi	bcc	3.572	3.526	0.793	0.804	1.40	[24]
CoCrCuFeNi	bcc	3.579	3.544	0.795	0.804	1.08	[24]
FeCrMnNiCo	bcc	3.590	3.595	0.802	0.804	0.35	[7]
FeCrMnNiCoNb	bcc	3.620	3.690	0.811	0.806	0.67	[7]
FeCrMnNiCoCu	bcc	3.590	3.570	0.803	0.804	0.17	[7]
FeCrMnNiCoV	bcc	3.580	3.581	0.810	0.804	0.63	[7]
W _{27.3} Nb _{22.7} Mo _{25.6} Ta _{24.4}	bcc	3.213	3.223	0.537	0.536	0.21	[10]
W _{21.1} Nb _{20.6} Mo _{21.7} Ta _{15.6} V ₂₁	bcc	3.183	3.182	0.535	0.536	0.20	[10]
Al _{0.4} Hf _{0.6} NbTaTiZr	bcc	3.367	3.438	0.546	0.537	1.79	[47]
HfNbTaTiZr	bcc	3.404	3.465	0.545	0.537	1.44	[48]

With Eqs. (5–7), a self-contained geometric model is developed, enabling the calculation of the intrinsic residual strains around the individual elements in a multicomponent alloy. Next, our goal is to verify whether these residual strains could be correlated with the phase stability in the multicomponent alloys. As inspired by the Lindemann's criterion [27,28], here we propose that, if there were really such a correlation, phase stability in a multicomponent alloy should be correlated with the root mean square (R.M.S.) residual strain, i.e. $\langle \varepsilon^2 \rangle = \sum_{j=1}^n c_j \varepsilon_j^2$ given that $\langle \varepsilon \rangle = \sum_{j=1}^n c_j \varepsilon_j = 0$. Literally, the R.M.S. residual strain measures the degree of fluctuation in the intrinsic residual strains from their mean value; however, it is worthy to point out that the R.M.S. residual strain is also related to the elastic energy stored in a multicomponent alloy. In theory, the total elastic energy stored in an alloy can be expressed as $U_e = \sum_{i=1}^n \frac{9}{2} K_i \varepsilon_i^2 V_i$, where K_i and V_i denote the bulk modulus and volume of the i th element, respectively. On the other hand, we may also write $U_e = \frac{9}{2} \bar{K} u_e V$, where \bar{K} is the average bulk modulus of the alloy, u_e the dimensionless elastic energy storage and V the total volume of the alloy. Equating the above two expressions for U_e then gives $u_e = \sum_{i=1}^n \alpha_i \beta_i c_i \varepsilon_i^2$ where $\alpha_i = \left(\frac{V_i}{\bar{V}}\right)^3$, $\beta_i = \frac{K_i}{\bar{K}}$ and \bar{V} is the average atomic radius of the alloy. Comparing u_e and

$\langle \varepsilon^2 \rangle$, it can be seen that the functional form for the R.M.S. residual strain is similar to that for the dimensionless elastic energy storage $\sqrt{u_e}$ except the difference in the weighting factors.

3. Lattice instability and phase transition in multicomponent alloys

3.1. Comparison with experimental data

To check if the phase stability in multicomponent alloys is correlated with the residual strains obtained from our geometric model, we first choose bulk metallic glasses as the model material. According to the previous research, it is already known that the glass forming ability of many alloys is strongly affected by the sizes of their constituent atoms due to the resultant excessive intrinsic residual strains [3–5,29]. Therefore, we expect that there should be a relatively high R.M.S. residual strain in the glass forming alloys if they assume a simple solid solution crystalline structure. To verify this, we calculated the R.M.S. residual strain in these typical glass-forming alloys with their compositions given in Refs. [30–32] and equilibrium packing fraction given by Eq. (7). The R.M.S. residual strains so obtained together with the corresponding

Table II. The summary of the mean-square residual strain $\langle \varepsilon^2 \rangle$, the root-mean-square residual strain $\sqrt{\langle \varepsilon^2 \rangle}$, the dimensionless elastic energy storage u_e and its root $\sqrt{u_e}$ calculated for a variety of typical glass forming alloys, including Cu-, Mg-, Zr-, La-, Nd-, Cu-, Ti- and Pd-based alloys. Data of composition are taken from Refs. [30–32]. Note that the heat of mixing ΔH for each alloy is also listed in the table for comparison.

Composition	$\langle \varepsilon^2 \rangle$	$\sqrt{\langle \varepsilon^2 \rangle}$	u_e	$\sqrt{u_e}$	ΔH (kJ/mol)
Cu ₄₆ Zr ₅₄	0.012830	0.1133	0.011885	0.1090	-22.85
Cu ₅₀ Zr ₅₀	0.013071	0.1143	0.012111	0.1101	-23.00
Cu _{64.5} Zr _{35.5}	0.012515	0.1119	0.011696	0.1082	-21.07
Mg ₈₀ Ni ₁₀ Nd ₁₀	0.005235	0.0724	0.007652	0.0875	-4.40
Mg ₇₅ Ni ₁₅ Nd ₁₀	0.007522	0.0867	0.009860	0.0993	-5.40
Mg ₇₀ Ni ₁₅ Nd ₁₅	0.007625	0.0873	0.010016	0.1001	-6.90
Mg ₆₅ Ni ₂₀ Nd ₁₅	0.009725	0.0986	0.011556	0.1075	-8.02
Mg ₆₅ Cu ₂₅ Y ₁₀	0.011434	0.1069	0.012437	0.1115	-7.16
Zr ₆₆ Al ₈ Ni ₂₆	0.011451	0.1070	0.011183	0.1058	-44.76
Zr ₆₆ Al ₈ Cu ₇ Ni ₁₉	0.010895	0.1044	0.010646	0.1032	-39.27
Zr ₆₆ Al ₈ Cu ₁₂ Ni ₁₄	0.010496	0.1025	0.010237	0.1012	-35.44
Zr ₆₆ Al ₉ Cu ₁₆ Ni ₉	0.009865	0.0993	0.009631	0.0981	-32.35
Zr ₆₅ Al _{7.5} Cu _{17.5} Ni ₁₀	0.010500	0.1025	0.010157	0.1008	-32.22
Zr ₅₇ Ti ₅ Al ₁₀ Cu ₂₀ Ni ₈	0.010147	0.1007	0.009776	0.0989	-31.51
Zr _{38.5} Ti _{16.5} Ni _{9.75} Cu _{15.25} Be ₂₀	0.019313	0.1390	0.016384	0.1280	-33.20
Zr _{39.88} Ti _{15.12} Ni _{9.98} Cu _{13.77} Be _{21.25}	0.020034	0.1415	0.017020	0.1305	-34.27
Zr _{41.2} Ti _{13.8} Cu _{12.5} Ni ₁₀ Be _{22.5}	0.020730	0.1440	0.017652	0.1329	-36.92
Zr _{42.63} Ti _{12.37} Cu _{11.25} Ni ₁₀ Be _{23.75}	0.021451	0.1465	0.018309	0.1353	-36.69
Zr ₄₄ Ti ₁₁ Cu ₁₀ Ni ₁₀ Be ₂₅	0.022159	0.1489	0.018961	0.1377	-37.07
Zr _{45.38} Ti _{9.62} Cu _{8.75} Ni ₁₀ Be _{26.25}	0.022871	0.1512	0.019636	0.1401	-38.00
Zr _{46.25} Ti _{8.25} Cu _{7.5} Ni ₁₀ Be _{27.5}	0.023614	0.1537	0.020363	0.1427	-38.94
La ₅₅ Al ₂₅ Ni ₂₀	0.029663	0.1722	0.023827	0.1544	-37.18
La ₅₅ Al ₂₅ Ni ₁₅ Cu ₅	0.029050	0.1704	0.023458	0.1532	-35.35
La ₅₅ Al ₂₅ Ni ₁₀ Cu ₁₀	0.028436	0.1686	0.023043	0.1518	-33.60
La ₅₅ Al ₂₅ Ni ₅ Cu ₁₅	0.027822	0.1668	0.022632	0.1504	-31.93
La ₅₅ Al ₂₅ Cu ₂₀	0.027209	0.1650	0.022168	0.1489	-30.34
La ₅₅ Al ₂₅ Ni ₅ Cu ₁₀ Co ₅	0.028335	0.1683	0.022989	0.1516	-32.31
La ₆₆ Al ₁₄ Cu ₂₀	0.025728	0.1604	0.022061	0.1485	-25.24
Nd ₆₀ Al ₁₅ Ni ₁₀ Cu ₁₀ Fe ₅	0.012486	0.1117	0.012385	0.1113	-27.37
Nd ₆₁ Al ₁₁ Ni ₈ Co ₅ Cu ₁₅	0.012946	0.1138	0.012627	0.1124	-19.54
Cu ₆₀ Zr ₃₀ Ti ₁₀	0.011189	0.1058	0.010428	0.1021	-18.72
Cu ₅₄ Zr ₂₇ Ti ₉ Be ₁₀	0.014056	0.1186	0.012708	0.1127	-20.89
Ti ₃₄ Zr ₁₁ Cu ₄₇ Ni ₈	0.007454	0.0863	0.007068	0.0841	-15.44
Pd ₄₀ Cu ₃₀ Ni ₁₀ P ₂₀	0.008704	0.0933	0.005789	0.0761	-24.88
Pd ₄₀ Ni ₄₀ P ₂₀	0.008802	0.0938	0.006322	0.0795	-26.24

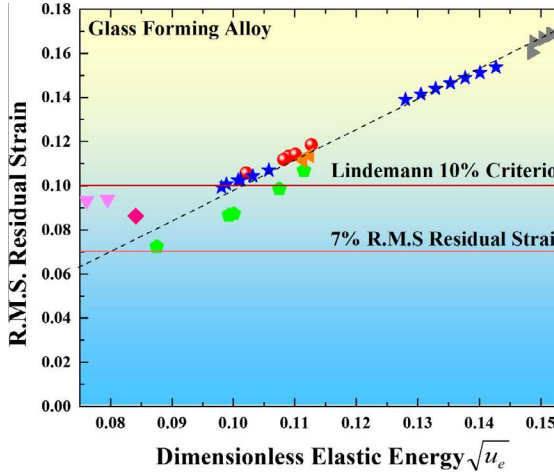


Fig. 3. The R.M.S. residual strain versus the dimensionless elastic energy as computed with our topological model for the typical glass forming alloys, including Cu-, Mg-, Zr-, La-, Nd-, Ti- and Pd-based bulk metallic glasses.

dimensionless elastic energies (please see [Appendix A.2](#) for the details) are listed in [Table II](#) and also plotted in [Fig. 3](#). As shown in [Fig. 3](#), there is a clear trend that the R.M.S. residual strains obtained from our geometric model increase with the dimensionless elastic energy stored in these glass-forming alloys. Within our expectation, this confirms that the R.M.S. residual strain can be regarded as equivalent to the normalized elastic energy storage. Furthermore, it can be noticed that, for these glass forming alloys, the obtained R.M.S. residual strains are relatively high, most of which are above a critical value of $\sim 10\%$. According to the Lindemann's criterion [[27,28](#)], lattice instability in a solid occurs once the R.M.S. vibrational amplitude of atoms exceeds $\sim 10\%$ of the average atomic size, which subsequently causes a solid–liquid transition. Here, if one takes the R.M.S. residual strain to be equal to the R.M.S. vibrational amplitude normalized by the atomic size, the 10% R.M.S. residual strain as obtained from the experimental data is then consistent very well with the Lindemann's criterion. By comparison, there are also a few glass-forming alloys, such as Mg- and Ti-based, exhibiting the R.M.S. residual strain of $\sim 7\%$, slightly lower than the Lindemann's criterion of $\sim 10\%$. Despite that, the general trend shown by the R.M.S. residual strains is encouraging and sensible ([Fig. 3](#)), implying that the Lindemann's criterion [[27,28](#)] might still work even for multicomponent alloys.

Next, let us consider HEAs which could be of single-phase solid solution, multi-phased or amorphous structure depending on their alloy compositions. Similarly, by assuming that HEAs form a solid solution crystalline structure, we could also calculate the R.M.S. residual strain and the dimensionless elastic energy for each alloy composition hitherto reported [[7,8,10,12,16,17,33–44](#)]. Here, it should be stressed that, for simplicity, there is no apparent VEC effect on the phase transition in the selected HEAs, as seen in [Table III](#). [Fig. 4](#) displays the calculation results showing a similar trend of the R.M.S. residual strain versus the dimensionless elastic energy with regard to the crystal-to-glass transition, namely, HEAs tend to form a glassy structure once their R.M.S. residual strain reaches above 10%.

More interestingly, it can be also seen from [Fig. 4](#) that the transition from a single-phase solid solution to a multi-phased structure takes place at the R.M.S. residual strain of about $\sim 5\%$, which is only one half of the Lindemann's criterion.

3.2. Geometric origin of phase transition

To rationalize our above findings, let us turn back to [Eq. \(4\)](#), the general expression for the residual strain ε_i that involves not only close atomic packing in a stable lattice but also the possible disturbance to the local lattice structure, as reflected by the relative change $\delta N_i/N_i$ in the CN of the central atom i . In our previous analysis, we assume a stable solid solution lattice and therefore neglect the possible effect of the change in CN. However, when a single-phase crystalline lattice, such as fcc, is about to transit either to another type of lattice or to an amorphous structure, it can be envisaged that some local change in the CN of constituent atoms may take place prior to the break-down of the overall lattice. This implies that, although the average residual strain still remains zero just before the phase transition, we should take into account the term $\delta N_i/N_i$ when calculating the intrinsic residual strain ε_i . Now, let us denote the residual strain with and without considering the CN effect to be ε_i^* and ε_i , respectively. Then it can be readily shown that:

$$\varepsilon_i^* - \varepsilon_i = \frac{\delta N_i}{N_i} \frac{\sum_{j=1}^n \omega_{ij} c_j}{\sum_{k=1}^n A_{ik} c_k} \quad (8)$$

Note that [Eq. \(8\)](#) is derived given the other parameters remaining unaltered (please see [Appendix A.3](#)). Since the mean of the residual strains should keep to zero, i.e. $\langle \varepsilon_i^* \rangle = \langle \varepsilon_i \rangle = 0$, irrespective of the CN change, we can then derive that ([Appendix A.3](#)):

$$\langle \varepsilon_i^{*2} \rangle + \langle \varepsilon_i^2 \rangle = \sum_i c_i \zeta_i \left(\frac{\delta N_i}{N_i} \right)^2 \quad (9)$$

where $\zeta_i = \left(\frac{\sum_{j=1}^n \omega_{ij} c_j}{\sum_{k=1}^n A_{ik} c_k} \right)^2$. Since the value of ζ_i is very close to unity (see [Appendix A.3](#)), [Eq. \(9\)](#) can be hence simplified to:

$$\langle (\varepsilon^*)^2 \rangle + \langle \varepsilon^2 \rangle \approx \left\langle \left(\frac{\delta N}{N} \right)^2 \right\rangle \quad (10)$$

Note that [Eq. \(10\)](#) has very important physical implications. In line with the atomic stress theory [[3–5](#)], we can propose that the lattice instability is triggered once the average change in the CN of the fcc lattice is about 1, or

$\sqrt{\langle (\delta N/N)^2 \rangle} \sim 1/12$. Now let us consider two limiting cases for what would happen upon the occurrence of lattice instability. Case I: most of the stored elastic strain energy is relaxed and hence $\langle (\varepsilon^*)^2 \rangle / \langle \varepsilon^2 \rangle \ll 1$. As a result, [Eq. \(10\)](#) is simplified to $\sqrt{\langle \varepsilon^2 \rangle} \approx 1/12 = 0.083$. Case II: only a small portion of the stored elastic strain energy is relaxed and therefore $\langle (\varepsilon^*)^2 \rangle \sim \langle \varepsilon^2 \rangle$. Consequently, we have $\sqrt{\langle \varepsilon^2 \rangle} \approx \frac{1}{12\sqrt{2}} \approx 0.059$. Comparing our theoretical predictions with the experimental data, it can be then inferred that the 10% R.M.S. residual strain, as extracted from the

Table III. The summary of the mean-square residual strain $\langle \varepsilon^2 \rangle$, the root-mean-square residual strain $\sqrt{\langle \varepsilon^2 \rangle}$, the dimensionless elastic energy storage u_e and its root $\sqrt{u_e}$ calculated for a variety of high entropy alloys. Note that the heat of mixing ΔH and VEC for each alloy is also listed in the table for comparison.

Composition	Phase	$\langle \varepsilon^2 \rangle$	$\sqrt{\langle \varepsilon^2 \rangle}$	u_e	$\sqrt{u_e}$	ΔH (kJ/mol)	VEC
CoCrCu _{0.5} FeNi [33]	fcc	0.000069	0.0083	0.000063	0.0079	0.49	8.56
FeCoNiCrCu [34]	fcc	0.000106	0.0103	0.000098	0.0099	3.20	8.8
FeNi ₂ CrCuAl _{0.2} [16]	fcc	0.000837	0.0289	0.000614	0.0248	0.12	8.77
CoCrFeMnNi [7]	fcc	0.001055	0.0325	0.000967	0.0311	-4.16	8
FeCoNiCrCuAl _{0.3} [34]	fcc	0.001138	0.0337	0.000829	0.0288	0.16	8.47
FeCoNiCrCuAl _{0.5} [34]	fcc	0.001693	0.0411	0.001242	0.0352	-1.52	8.27
FeNi ₂ CrCuAl _{0.6} [16]	fcc	0.001965	0.0443	0.001455	0.0381	-3.27	8.36
Al _{0.5} CoCrCuFeNiTi _{0.2} [35]	fcc	0.002372	0.0487	0.002015	0.0449	-4.15	8.12
Al _{0.3} CoCrFeNi [36]	fcc	0.001368	0.0370	0.000950	0.0308	-7.27	7.88
Al _{0.5} CrCuFeNi ₂ [37]	fcc	0.001717	0.0414	0.001265	0.0356	-2.51	8.45
VCuFeCoNi [17]	fcc	0.000483	0.0220	0.000506	0.0225	-2.24	8.6
WNbMoTa [10]	bcc	0.000534	0.0231	0.000522	0.0228	-6.50	5.5
WNbMoTaV [10]	bcc	0.000995	0.0315	0.000829	0.0288	-4.64	5.4
CrCuFeMnNi [38]	bcc	0.001013	0.0318	0.000970	0.0311	2.72	8.4
AlCo ₃ CrCu _{0.5} FeNi [35]	Multi	0.002327	0.0482	0.001676	0.0409	-7.25	7.93
FeCoNiCrCuAl _{0.8} [34]	Multi	0.002368	0.0487	0.001772	0.0421	-3.61	8
Al _{0.8} CrCuFeMnNi [38]	Multi	0.002621	0.0512	0.002198	0.0469	-3.97	7.66
AlCo ₂ CrCu _{0.5} FeNi [35]	Multi	0.002616	0.0511	0.001920	0.0438	-7.67	7.77
FeCoNiCrCuAl [34]	Multi	0.002734	0.0523	0.002073	0.0455	-4.78	7.83
FeNi ₂ CrCuAl [16]	Multi	0.002771	0.0526	0.002107	0.0459	-5.78	8
AlCrCuFeMnNi [38]	Multi	0.002876	0.0536	0.002417	0.0492	-5.11	7.5
FeNi ₂ CrCuAl ₂ [16]	Multi	0.003085	0.0555	0.002377	0.0488	-6.78	7.84
FeCoNiCrCuAl _{1.5} [34]	Multi	0.003424	0.0585	0.002685	0.0518	-7.05	7.46
CuAlNiCoCrFeSi [39]	Multi	0.003723	0.0610	0.002637	0.0513	-18.86	7.29
FeCoNiCrCuAl _{2.0} [34]	Multi	0.003880	0.0623	0.003140	0.0560	-8.65	7.14
FeCoNiCrCuAl _{2.3} [34]	Multi	0.004074	0.0638	0.003355	0.0579	-9.38	6.97
FeCoNiCrCuAl _{2.8} [34]	Multi	0.004301	0.0656	0.003640	0.0603	-10.28	6.71
FeCoNiCrCuAl ₃ [34]	Multi	0.004365	0.0661	0.003732	0.0611	-10.56	6.63
CuCoNiCrAlFeTiV [12]	Multi	0.003979	0.0631	0.003686	0.0607	-13.94	7
Al _{0.5} CoCrFeNi [36]	Multi	0.002061	0.0454	0.001463	0.0382	-9.09	7.67
Al _{0.5} CoCrCuFeNiTi _{0.4} [35]	Multi	0.002948	0.0543	0.002662	0.0516	-6.42	7.98
Al _{0.5} CrFeNiCoCuTi _{0.6} [35]	Multi	0.003437	0.0586	0.003206	0.0566	-8.40	7.85
Al _{0.5} CrFeNiCoCuTi _{0.8} [35]	Multi	0.003853	0.0621	0.003662	0.0605	-10.11	7.73
Al _{0.5} CoCrCuFeNiTi _{1.0} [35]	Multi	0.004206	0.0649	0.004047	0.0636	-11.60	7.62
Al _{0.5} CoCrCuFeNiTi _{1.2} [35]	Multi	0.004507	0.0671	0.004371	0.0661	-12.89	7.51
Al _{0.5} CoCrCuFeNiTi _{1.4} [35]	Multi	0.004763	0.0690	0.004644	0.0681	-14.02	7.41
Al _{0.5} CoCrCuFeNiTi _{1.6} [35]	Multi	0.004980	0.0706	0.004873	0.0698	-15.01	7.31
Al _{0.5} CoCrCuFeNiTi _{1.8} [35]	Multi	0.005164	0.0719	0.005065	0.0712	-15.86	7.22
Al _{0.5} CoCrCuFeNiTi _{2.0} [35]	Multi	0.005318	0.0729	0.005225	0.0723	-16.60	7.13
CoCrFeNiTi _{0.5} [37]	Multi	0.002758	0.0525	0.002783	0.0528	-11.56	7.78
FeCoNiCuAl [40]	Multi	0.003095	0.0556	0.002381	0.0488	-5.28	8.2
CoCrFeNiAlNb _{0.25} [17]	Multi	0.003665	0.0605	0.003186	0.0564	-14.66	7.1
CoCrFeNiAlNb _{0.75} [17]	Multi	0.004193	0.0648	0.004104	0.0641	-18.03	6.91
PdPtCuNiP [8]	Amorphous	0.009068	0.0952	0.006857	0.0828	-23.68	9.2
TiZrCuNiBe [41]	Amorphous	0.016083	0.1268	0.014185	0.1191	-30.24	6.2
TiZrHfCuNi [42]	Amorphous	0.011006	0.1049	0.010380	0.1019	-27.36	6.6
SrCaYbMgZn [43]	Amorphous	0.024489	0.1565	0.018829	0.1372	-13.12	4.2
ErTbDyNiAl [44]	Amorphous	0.020409	0.1429	0.018654	0.1366	-37.60	4.4
SrCaYbMgZn _{0.5} Cu _{0.5} [44]	Amorphous	0.028856	0.1699	0.022479	0.1499	-10.60	4.1
SrCaYbLi _{0.55} Mg _{0.45} Zn [44]	Amorphous	0.025969	0.1612	0.021255	0.1458	-12.15	4.09

data of crystal-to-glass transition, signals the full stress relaxation while the 5% R.M.S. residual strain, as extracted from the data of single- to multi-phase transition, hints only a partial relaxation of the residual strain. Physically, this makes sense since amorphous structures have many possible metastable configurations. Therefore, residual strains in the otherwise crystalline lattice can be easily released through structural relaxation after phase transition. In contrast, a multi-phased structure retains, at least partially, the original lattice structure with newly formed

phase boundaries. As a result, the residual strains and the resultant elastic energy cannot be fully released as in an amorphous structure. In such a sense, it is natural that the critical R.M.S. residual strain for single- to multi-phase transition is lower than that for crystal to glass transition in HEAs. Based on the above discussions, it can be seen that our theoretical modeling is quite promising as it is in good agreement with the data obtained from so many experiments carried out by different research groups, as referenced in Tables I–III.

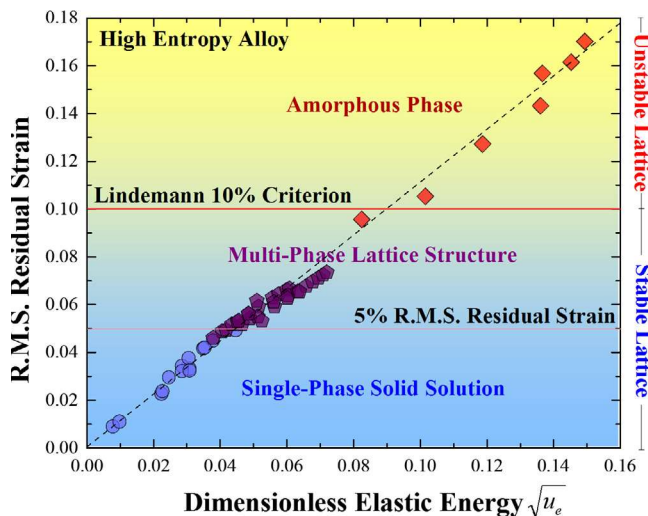


Fig. 4. The R.M.S. residual strain versus the dimensionless elastic energy as computed with our topological model for different types of HEAs.

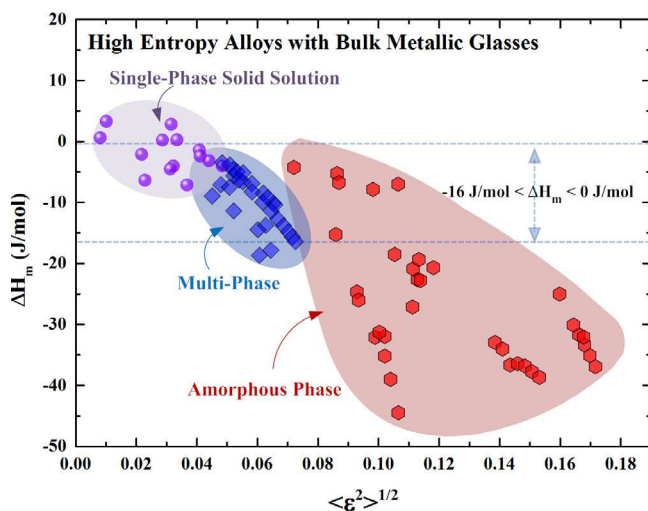


Fig. 5. The plot of the heat of mixing ΔH_m versus the R.M.S. residual strain $\langle \varepsilon^2 \rangle^{1/2}$ for high entropy alloys and bulk metallic glasses. Data are taken from Table II and III.

4. Implication

Before conclusion, let us discuss one important implication of the current work. Fig. 5 shows the plot of the R.M.S. residual strain $\langle \varepsilon^2 \rangle^{1/2}$ versus the heat of mixing ΔH_m obtained from different types of HEAs and bulk metallic glasses. Evidently, a general trend can be perceived from this figure that the lower is the heat of mixing ΔH_m , the higher is the R.M.S. residual strain $\langle \varepsilon^2 \rangle^{1/2}$, particularly so for bulk metallic glasses. Since the magnitude of the R.M.S. residual strain can be generally correlated with the normalized elastic energy storage and the degree of lattice instability, this trend suggests that the formation of bulk metallic glasses is favored at a lower ΔH_m (negative) with a higher tendency of glass forming. In general this is consistent with the Inoue's empirical laws [45] and many others [3–5,9,29], which simply states that glass formation

is strongly affected by the topology of the atomic structure as well as the chemistry. However, it is worthy to point out that the phase transition in multicomponent alloys, such as the single- to multi-phase and crystal-to-glass transition, seems less dependent on the heat of mixing ΔH_m in the boundary regions that separate different phases. As indicated in Fig. 5, there is a significant overlap in ΔH_m between different phases when approaching the point of the phase transition, which implies that the phase transition in many multicomponent alloys is more of a geometric than chemical origin. This is a very interesting finding but we should be cautious in the interpretation. In principle, it is the free energy that governs the phase transition in multicomponent alloys; therefore, both chemistry and geometry should be important. One possible reason that may explain our current finding is that, with more elements being mixed together, the average bonding in the multicomponent alloys is more of a metallic type; therefore, local chemical short-range order, such as the formation of intermetallic clusters, plays a lesser role than the atomic size effect in the borderline cases in which the alloy can barely transform from one phase to another upon solidification. To verify this thinking, more research work is certainly needed which will be addressed in our future work.

5. Concluding remarks

To conclude, a simple self-contained geometric model is developed in this work to calculate the intrinsic residual strains in the HEAs as well as in other types of alloys. To obtain the intrinsic residual strains in an existing alloy, one may use an experimentally determined lattice constant as the input in the calculation or he may also employ the ideal atomic packing fraction as an approximation to predict the intrinsic residual strains in the alloy to be designed. Based on our analyses and findings, some salient conclusions are drawn, as listed below:

- (1) As verified on glass forming alloys and HEAs, the crystal-to-glass transition is correlated with the R.M.S. residual strain of $\sim 10\%$, being in line with the Lindemann's criterion for lattice instability.
- (2) According to the experimental data of HEAs, the transition from a single phase solid solution to multi-phased structure is correlated with the R.M.S. residual strain of $\sim 5\%$.
- (3) Theoretically, the 10% R.M.S. residual strain can be related to a full release of the elastic energy upon phase transition while the 5% R.M.S. residual strain only to a partial release.
- (4) Regardless of the chemical complexity of multicomponent alloys, our theoretical modeling, when compared with the existing experimental data, suggests that, upon solidification, single phase solid solution prevails in as-cast HEAs when their R.M.S. residual strain is less than 5% or amorphous structure prevails when their R.M.S. residual strain is above 10%. In between, the as-cast HEAs tend to form multi-phased structures.

Finally, we would point out again that, due to the neglect of the chemistry effect, our theoretical model only provides an estimation of the intrinsic residual strains in the multicomponent alloys. Nevertheless, our current findings are still important as they shed a quantitative and

physical insight into the geometric origin of phase transition in these alloys. Particularly, the approach we developed here should be very useful in the initial screening of alloy composition in the design of HEAs as well as that of conventional alloys.

Acknowledgments

Y.Y. and C.T.L. are thankful to the financial support provided by the Research Grant Council (RGC), the Hong Kong government, through the general research fund (GRF) with the account number of CityU11214914 and CityU117612, respectively.

Appendix A.1

Assuming that an equilibrium atomic packing efficiency $\bar{\eta}$ is obtained after the development of the intrinsic residual strain, we can derive the following general equation:

$$\bar{\eta} = \bar{\eta}_i + \delta\bar{\eta}_i = \frac{N_i \sum_{j=1}^n c_j \omega_{ij} + N_i \sum_{j=1}^n c_j \delta\omega_{ij} + \delta N_i \sum_{j=1}^n c_j \omega_{ij}}{4\pi} \quad (\text{A1})$$

where $\delta\bar{\eta}_i$ denotes the incremental change of the atomic packing efficiency; δN_i denotes the change in the CN of the i th atom and $\delta\omega_{ij} = -A_{ij}(\varepsilon_i - \varepsilon_j)$, in which $A_{ij} = \frac{2\pi x_{ij}}{(x_{ij}+1)^2 \sqrt{x_{ij}(x_{ij}+2)}}$ and the intrinsic residual strain $\varepsilon_i = \frac{\delta r_i}{r_i}$.

Appendix A.2

In principle, the total elastic energy stored in an alloy can be generally expressed as $U_e = \sum_{i=1}^n \frac{9}{2} K_i \varepsilon_i^2 V_i$, where K_i and V_i denote the bulk modulus and total volume of the i th element, respectively. Meanwhile, we may also write $U_e = \frac{9}{2} \bar{K} u_e V$, where $\bar{K} = \sum_{i=1}^n c_i K_i$ is the average bulk modulus of the alloy, u_e the dimensionless elastic energy storage and V the total volume of the alloy. Note that the bulk modulus of different elements used for the theoretical calculation was taken from Ref. [46]. Equating the above two expressions for U_e gives $u_e = \sum_{i=1}^n \alpha_i \beta_i c_i \varepsilon_i^2$, where $\alpha_i = \left(\frac{r_i}{\bar{r}}\right)^3$, $\beta_i = \frac{K_i}{\bar{K}}$ and $\bar{r} = \sum_{i=1}^n c_i r_i$ is the average atomic radius of the alloy.

Appendix A.3

When taking the CN effect into consideration, the residual strain ε_i^* is given in the form of Eq. (4); by comparison, the residual strain ε_i is given in the form of Eq. (5) when neglecting the CN effect. Taking other parameters to be identical, subtracting Eq. (5) from Eq. (4) gives:

$$\varepsilon_i^* - \varepsilon_i = \frac{\delta N_i}{N_i} \frac{\sum_{j=1}^n \omega_{ij} c_j}{\sum_{k=1}^n A_{ik} c_k} \quad (\text{A2})$$

With Eq. (A2), we can further derive:

$$\sum_{i=1}^n c_i (\varepsilon_i^* - \varepsilon_i)^2 = \sum_{i=1}^n c_i \zeta_i \left(\frac{\delta N_i}{N_i} \right)^2 \quad (\text{A3})$$

where $\zeta_i = \left(\frac{\sum_{j=1}^n \omega_{ij} c_j}{\sum_{k=1}^n A_{ik} c_k} \right)^2$. Since $\langle \varepsilon_i^* \rangle = \langle \varepsilon_i \rangle = 0$ and ε_i^* and ε_i are statistically independent, we should have $\langle \varepsilon_i^* \varepsilon_i \rangle = 0$. Therefore, Eq. (A4) could be simplified to:

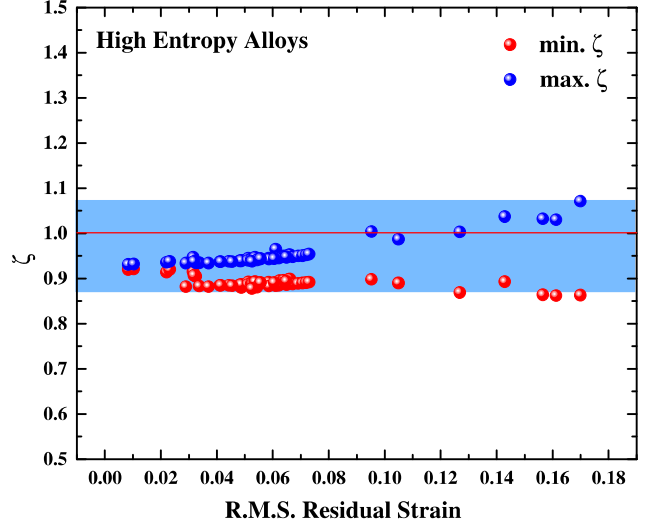


Fig. A1. The minimum and maximum ζ_i obtained from HEAs with different R.M.S. residual strain.

$$\langle \varepsilon_i^{*2} \rangle + \langle \varepsilon_i^2 \rangle = \sum_{i=1}^n c_i \zeta_i \left(\frac{\delta N_i}{N_i} \right)^2 \quad (\text{A4})$$

As seen in Fig. A1, the possible values of ζ_i as obtained from a variety of HEAs fall into a very narrow range between 0.9 and 1.0. In such a case, Eq. (A4) could be further simplified as:

$$\langle (\varepsilon^*)^2 \rangle + \langle \varepsilon^2 \rangle \approx \left\langle \left(\frac{\delta N}{N} \right)^2 \right\rangle \quad (\text{A5})$$

References

- [1] U. Mizutani, Hume-Rothery Rules for Structurally Complex Alloy Phases, CRC Press, 2010.
- [2] J.D. Eshelby, The continuum theory of lattice defects, in: S. Frederick, T. David (Eds.), Solid State Physics, Academic Press, 1956, pp. 79–144.
- [3] T. Egami, Universal criterion for metallic glass formation, Mater. Sci. Eng., A 226–228 (1997) 261–267.
- [4] T. Egami, Atomic level stresses, Prog. Mater Sci. 56 (2011) 637–653.
- [5] T. Egami, Y. Waseda, Atomic size effect on the formability of metallic glasses, J. Non-Cryst. Solids 64 (1984) 113–134.
- [6] Y. Zhang, T.T. Zuo, Z. Tang, M.C. Gao, K.A. Dahmen, P.K. Liaw, et al., Microstructures and properties of high-entropy alloys, Prog. Mater Sci. 61 (2014) 1–93.
- [7] B. Cantor, I.T.H. Chang, P. Knight, A.J.B. Vincent, Microstructural development in equiatomic multicomponent alloys, Mater. Sci. Eng., A 375–377 (2004) 213–218.
- [8] A. Takeuchi, N. Chen, T. Wada, Y. Yokoyama, H. Kato, A. Inoue, et al., $Pd_{20}Pt_{20}Cu_{20}Ni_{20}P_{20}$ high-entropy alloy as a bulk metallic glass in the centimeter, Intermetallics 19 (2011) 1546–1554.
- [9] A. Takeuchi, K. Amiya, T. Wada, K. Yubuta, W. Zhang, A. Makino, Entropies in alloy design for high-entropy and bulk glassy alloys, Entropy 15 (2013) 3810–3821.
- [10] O.N. Senkov, G.B. Wilks, D.B. Miracle, C.P. Chuang, P.K. Liaw, Refractory high-entropy alloys, Intermetallics 18 (2010) 1758–1765.
- [11] Y.F. Ye, Q. Wang, J. Lu, C.T. Liu, Y. Yang, The generalized thermodynamic rule for phase selection in multicomponent alloys, Intermetallics 59 (2015) 75–80.

- [12] J.W. Yeh, S.K. Chen, J.Y. Gan, S.J. Lin, T.S. Chin, T.T. Shun, et al., Formation of simple crystal structures in Cu–Co–Ni–Cr–Al–Fe–Ti–V alloys with multiprincipal metallic elements, *Metall. Mater. Trans. A* 35 A (2004) 2533–2536.
- [13] C. Ng, S. Guo, J. Luan, S. Shi, C.T. Liu, Entropy-driven phase stability and slow diffusion kinetics in an Al_{0.5}CoCrCuFeNi high entropy alloy, *Intermetallics* 31 (2012) 165–172.
- [14] W.H. Liu, Y. Wu, J.Y. He, Y. Zhang, C.T. Liu, Z.P. Lu, The phase competition and stability of high-entropy alloys, *JOM* 66 (2014) 1973–1983.
- [15] S. Guo, C.T. Liu, Phase stability in high entropy alloys: formation of solid-solution phase or amorphous phase, *Prog. Nat. Sci.: Mater. Int.* 21 (2011) 433–446.
- [16] S. Guo, C. Ng, J. Lu, C.T. Liu, Effect of valence electron concentration on stability of fcc or bcc phase in high entropy alloys, *J. Appl. Phys.* 109 (2011).
- [17] Y. Zhang, Y.J. Zhou, J.P. Lin, G.L. Chen, P.K. Liaw, Solid-solution phase formation rules for multi-component alloys, *Adv. Eng. Mater.* 10 (2008) 534–538.
- [18] Z. Wang, Y. Huang, Y. Yang, J. Wang, C.T. Liu, Atomic-size effect and solid solubility of multicomponent alloys, *Scripta Mater.* 94 (2015) 28–31.
- [19] Z. Liu, S. Guo, X. Liu, J. Ye, Y. Yang, X.-L. Wang, et al., Micromechanical characterization of casting-induced inhomogeneity in an Al_{0.8}CoCrCuFeNi high-entropy alloy, *Scripta Mater.* 64 (2011) 868–871.
- [20] H.W. King, Quantitative size-factors for metallic solid solutions, *J. Mater. Sci.* 1 (1966) 79–90.
- [21] G. Ungar, Y. Liu, X. Zeng, V. Percec, W.-D. Cho, Giant supramolecular liquid crystal lattice, *Science* 299 (2003) 1208–1211.
- [22] L. Vegard, Die konstitution der mischkristalle und die raumfüllung der atome, *Z Physik* 5 (1921) 17–26.
- [23] S.T. Murphy, A. Chroneos, C. Jiang, U. Schwingenschlögl, R.W. Grimes, Deviations from Vegard's law in ternary III–V alloys, *Phys. Rev. B* 82 (2010) 073201.
- [24] S. Guo, C. Ng, Z. Wang, C.T. Liu, Solid solutioning in equiatomic alloys: limit set by topological instability, *J. Alloy. Compd.* 583 (2014) 410–413.
- [25] V.A. Lubarda, On the effective lattice parameter of binary alloys, *Mech. Mater.* 35 (2003) 53–68.
- [26] W.B. Pearson, *A Handbook of Lattice Spacings and Structures of Metals and Alloys*, 1967.
- [27] F.A. Lindemann, The calculation of molecular vibration frequencies, *Physik Z* 11 (1910) 609–612.
- [28] D.W. Oxtoby, New perspectives on freezing and melting, *Nature* 347 (1990) 725–730.
- [29] O.N. Senkov, D.B. Miracle, Effect of the atomic size distribution on glass forming ability of amorphous metallic alloys, *Mater. Res. Bull.* 36 (2001) 2183–2198.
- [30] Z.P. Lu, C.T. Liu, A new glass-forming ability criterion for bulk metallic glasses, *Acta Mater.* 50 (2002) 3501–3512.
- [31] N. Nishiyama, A. Inoue, Direct comparison between critical cooling rate and some quantitative parameters for evaluation of glass-forming ability in Pd–Cu–Ni–P Alloys, *Mater. Trans., JIM* 43 (2002) 1913–1917.
- [32] M.I. Mendelev, M.J. Kramer, R.T. Ott, D.J. Sordellet, M.F. Besser, A. Kreyssig, et al., Experimental and computer simulation determination of the structural changes occurring through the liquid–glass transition in Cu–Zr alloys, *Phil. Mag.* 90 (2010) 3795–3815.
- [33] C.C. Tung, J.W. Yeh, T.T. Shun, S.K. Chen, Y.S. Huang, H.C. Chen, On the elemental effect of AlCoCrCuFeNi high-entropy alloy system, *Mater. Lett.* 61 (2007) 1–5.
- [34] C.J. Tong, Y.L. Chen, S.K. Chen, J.W. Yeh, T.T. Shun, C.H. Tsau, et al., Microstructure characterization of AlxCoCrCuFeNi high-entropy alloy system with multiprincipal elements, *Metall. Mater. Trans. A* 36 (2005) 881–893.
- [35] G.Y. Ke, S.K. Chen, T. Hsu, J.W. Yeh, FCC and BCC equivalents in as-cast solid solutions of Al_xCo_yCr_zCu_{0.5}Fe_w high-entropy alloys, *Ann. Chim.: Sci. Mater.* 31 (2006) 669–683.
- [36] Y.F. Kao, T.J. Chen, S.K. Chen, J.W. Yeh, Microstructure and mechanical property of as-cast, -homogenized, and -deformed Al_xCo_yCr_zFe_w ($0 \leq x \leq 2$) high-entropy alloys, *J. Alloy. Compd.* 488 (2009) 57–64.
- [37] L. Jiang, Y. Lu, Y. Dong, T. Wang, Z. Cao, T. Li, Annealing effects on the microstructure and properties of bulk high-entropy CoCrFeNiTi_{0.5} alloy casting ingot, *Intermetallics* 44 (2014) 37–43.
- [38] H.Y. Chen, C.W. Tsai, C.C. Tung, J.W. Yeh, T.T. Shun, C.C. Yang, et al., Effect of the substitution of Co by Mn in Al–Cr–Cu–Fe–Co–Ni high-entropy alloys, *Ann. Chim.: Sci. Mater.* 31 (2006) 685–698.
- [39] J.W. Yeh, S.Y. Chang, Y.D. Hong, S.K. Chen, S.J. Lin, Anomalous decrease in X-ray diffraction intensities of Cu–Ni–Al–Co–Cr–Fe–Si alloy systems with multi-principal elements, *Mater. Chem. Phys.* 103 (2007) 41–46.
- [40] Y.X. Zhuang, H.D. Xue, Z.Y. Chen, Z.Y. Hu, J.C. He, Effect of annealing treatment on microstructures and mechanical properties of FeCoNiCuAl high entropy alloys, *Mater. Sci. Eng., A* 572 (2013) 30–35.
- [41] H.Y. Ding, K.F. Yao, High entropy Ti₂₀Zr₂₀Cu₂₀Ni₂₀Be₂₀ bulk metallic glass, *J. Non-Cryst. Solids* 364 (2013) 9–12.
- [42] L. Ma, L. Wang, T. Zhang, A. Inoue, Bulk glass formation of Ti–Zr–Hf–Cu–M (M = Fe, Co, Ni) alloys, *Mater. Trans.* 43 (2002) 277–280.
- [43] H.F. Li, X.H. Xie, K. Zhao, Y.B. Wang, Y.F. Zheng, W.H. Wang, et al., In vitro and in vivo studies on biodegradable CaMgZnSrYb high-entropy bulk metallic glass, *Acta Biomater.* 9 (2013) 8561–8573.
- [44] X.Q. Gao, K. Zhao, H.B. Ke, D.W. Ding, W.H. Wang, H.Y. Bai, High mixing entropy bulk metallic glasses, *J. Non-Cryst. Solids* 357 (2011) 3557–3560.
- [45] A. Inoue, Stabilization of metallic supercooled liquid and bulk amorphous alloys, *Acta Mater.* 48 (2000) 279–306.
- [46] <http://periodictable.com/Properties/A/BulkModulus.html>.
- [47] O.N. Senkov, S.V. Senkova, C. Woodward, Effect of aluminum on the microstructure and properties of two refractory high-entropy alloys, *Acta Mater.* 68 (2014) 214–228.
- [48] O.N. Senkov, J.M. Scott, S.V. Senkova, D.B. Miracle, C.F. Woodward, Microstructure and room temperature properties of a high-entropy TaNbHfZrTi alloy, *J. Alloy. Compd.* 509 (2011) 6043–6048.